

COIN CDN 2012-1-55 - CU ALLOY - LATE ROMAN TIMES - SWITZERLAND

Artefact name Coin CdN 2012-1-55

Authors Naima. Gutknecht (HE-Arc CR, Neuchâtel, Neuchâtel, Switzerland) & Valentina. Valbi (Laboratoire Métallurgie et Culture (LMC), Belfort, Franche-Comté, France) & Rey-Bellet. Bernadette (Musée d'art et d'histoire, Genève, Genève, Geneva, Switzerland)

Url /artefacts/1340/

✖ The object



Fig. 1: Views of both sides of a coin from the "Peney hoard" with blue and green corrosion products,

Credit MAHG, B.Rey-Bellet.

✖ Description and visual observation

Description of the artefact Coin with blue and green corrosion products. Identification as Honorius, Western Roman Emperor (393-423). The coin is probably an imitation. Diameter: about 1.5cm.

Type of artefact coin

Origin Peney, Genève, Geneva, Switzerland

Recovering date 1960

Chronology category Late roman times

chronology tpq

chronology taq

Chronology comment

Burial conditions / environment Soil

Artefact location Musée d'art et d'histoire, Genève, Geneva

Owner	Musée d'art et d'histoire, Genève, Geneva
Inv. number	CdN 2012-1-55
Recorded conservation data	No conservation treatment reported.

Complementary information

Object recovered in 1960 at Peney, Geneva, Switzerland in a hoard containing 4000 coins. Around 1400 coins from the hoard are conserved at the Art and History Museum of Geneva.

Study area(s)

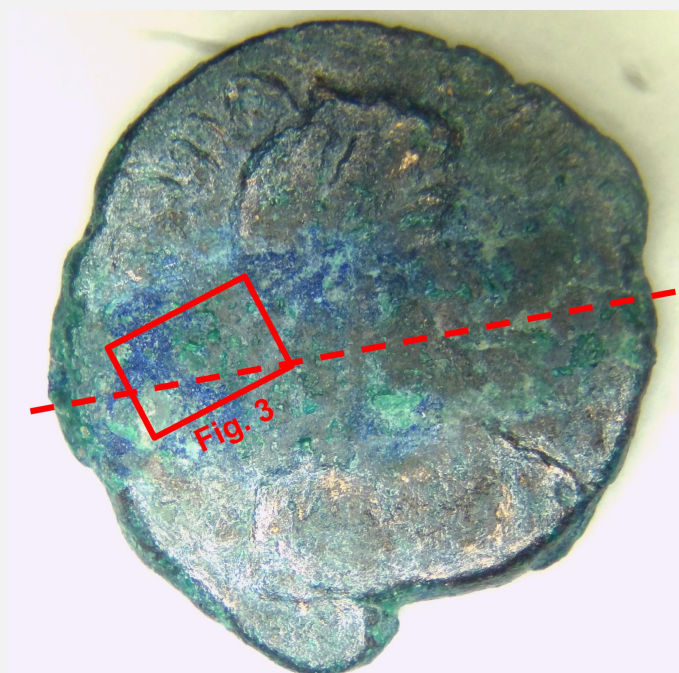


Fig. 2: Location of the detail (Fig. 3) and of the sampling for cross-section,

Credit MAHG, B.Rey-Bellet/ HE-Arc CR, N.Gutknecht.

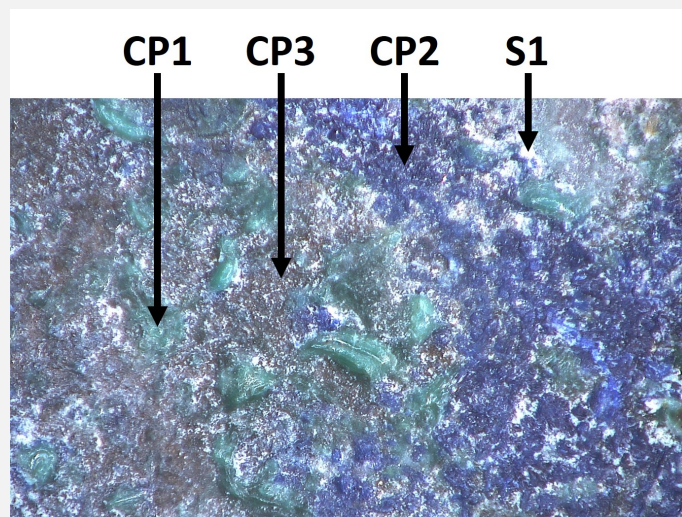


Fig. 3: Detail of the corrosion structure with reference to fig. 4,

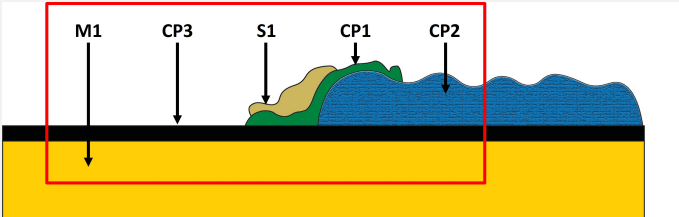
Credit MAHG, B.Rey-Bellet/HE-Arc CR, N.Gutknecht.

Binocular observation and representation of the corrosion structure

The schematic representation below gives an overview of the corrosion structure encountered on the coin from a first visual macroscopic observation.

Stratum	Type of stratum	Principal characteristics
S1	Soil	Cluster, light grey, thin, scattered, non-compact, soft
CP1	Corrosion product	Cluster, dark green, medium, scattered, compact, very soft
CP2	Corrosion product	Cluster, blue, medium, scattered, compact, very soft
CP3	Corrosion product	Layer, black, thin, continuous, compact, soft
M1	Metal	Dark yellow, metallic, soft

Table 1: Description of the principal characteristics of the strata as observed under binocular microscope according to Bertholon's method.



Credit HE-Arc CR, N.Gutknecht.

Fig. 4: Stratigraphic representation of the corrosion structure of the coin by macroscopic and binocular observation with indication of the corrosion structure used to build the MiCorr stratigraphy of Fig. 5 (red square),

✧ MiCorr stratigraphy(ies) – Bi

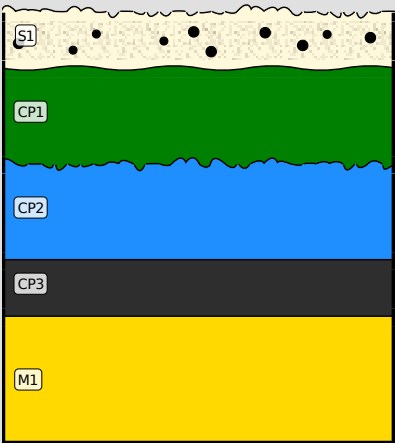


Fig. 5: Stratigraphic representation of the corrosion structure of the coin observed macroscopically under binocular microscope using the MiCorr application. The characteristics of the strata are only accessible by clicking on the drawing that redirects you to the search tool by stratigraphy representation, Credit MAHG, B.Rey-Bellet/HE-Arc CR, N.Gutknecht.

✧ Sample(s)



Credit LMC-CNRS, V.Valbi.

Fig. 6: Micrograph of the cross-section of the sample taken from the coin (Fig. 2) in dark field showing the location of Figs. 8 to 10,

Description of sample

The cross-section corresponds to a cut of the coin in half (Fig. 2) and is representative of the entire thickness of the coin's body. A metallic core is present below the corrosion layers (Fig. 6).

Alloy

Cu Alloy

Technology	Annealed after cold working
Lab number of sample	BL55
Sample location	Musée d'art et d'histoire, Genève, Geneva
Responsible institution	Musée d'art et d'histoire, Genève, Geneva
Date and aim of sampling	June 2021

Complementary information

None.

✧ Analyses and results

Analyses performed:

Non-invasive approach

- XRF with handheld portable X-ray fluorescence spectrometer (NITON XL3t 950 Air GOLDD+, Thermo Fischer®). General Metal mode, acquisition time 60s (filters: Li20/Lo20/M20).

Invasive approach (on the sample)

- Optical microscopy: the sample is polished, then it is observed with a numerical microscope KEYENCE VHX-7000 in bright and dark field.

- Metallography: the polished sample is etched with alcoholic ferric chloride and observed by optical microscopy in bright field.

- SEM-EDS: the sample is coated with a carbon layer and analyses are performed on a SEM-FEG JEOL 7001-F equipped with a silicon-drift EDS Oxford detector (Aztec analysis software) with an accelerating voltage of 20 kV and probe current at about 9 nA. The relative error is considered of about 10% for content range <1mass%, and of 2% for content range of >1mass%.

- μ -Raman spectroscopy: it is performed on a HORIBA Labram Xplora spectrometer equipped with a 532 nm laser with 1800 grating, the laser power employed is between 0.04 and 0.55 mW with acquisition time varying between 1 and 5 minutes.

✧ Non invasive analysis

The XRF analysis of coin CdN 2012-1-55 was carried out before sampling. All strata, from soil and corrosion products to metal, are analyzed at the same time. The metal is presumably a copper-lead-tin alloy, while the other elements detected (Fe, Si, Al) are from the environment.

Elements	mass %
Cu	69
Pb	25
Sn	1
Sb	<1
Fe	<1
Si	2
Al	2

Table 2: Chemical composition of the surface of coin CdN 2012-1-55. Method of analysis: XRF, General Metal mode, acquisition time 60s (filters: Li20/LO20/M20). The results are rounded up to the nearest whole number, UR-Arc CR.

EDX analysis (Table 3) of the residual metal on cross-section of sample BL55 indicates that it is a Cu-Pb-Sn ternary alloy with a high percentage of Pb (29 wt%). This confirms XRF analysis (Table 2).

Elements	wt%
Cu	67
Pb	29
Sn	2

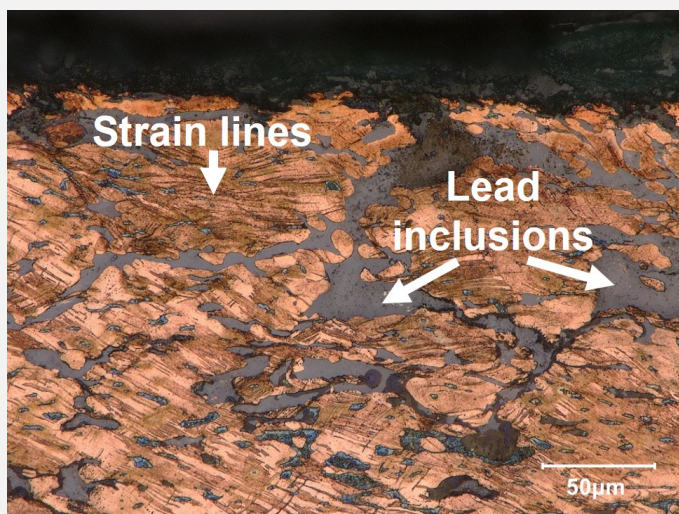
Table 3: Chemical composition (wt%) of the alloy over a general area of analysis, LMC-IRAMAT-CNRS-UTBM.

The sample presents on its whole thickness big Pb inclusions (50-100 μm , Figs. 7 and 8) homogeneously distributed. The metal has a polygonal grain structure (Figs. 8-9) with locally elongated grains and slip lines revealing that the object underwent cold working. Several longitudinal cracks are observed and are filled with corrosion products (Fig. 9).



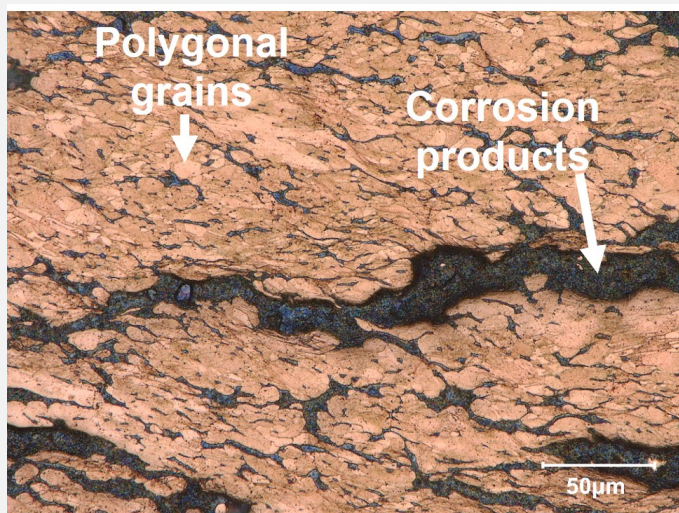
Credit LMC-CNRS, V.Valbi.

Fig. 7: Micrograph (similar to Fig. 6) of the cross-section of the sample taken from the coin (Fig. 2) in bright field after chemical etching,



Credit LMC-CNRS, V.Valbi.

Fig. 8: Micrograph of the metal sample from Fig. 7 (detail), etched, bright field. Elongated grains with slip lines are observed, as well as grey lead inclusions,



Credit LMC-CNRS, V.Valbi.

Fig. 9: Micrograph of the metal sample from Fig. 7 (detail), etched, bright field. with polygonal microstructure and presence of longitudinal crack filled with corrosion products (azurite, malachite),

Microstructure	Polygonal grains with inclusions
First metal element	Cu
Other metal elements	Sn, Pb

Complementary information

None.

Corrosion layers

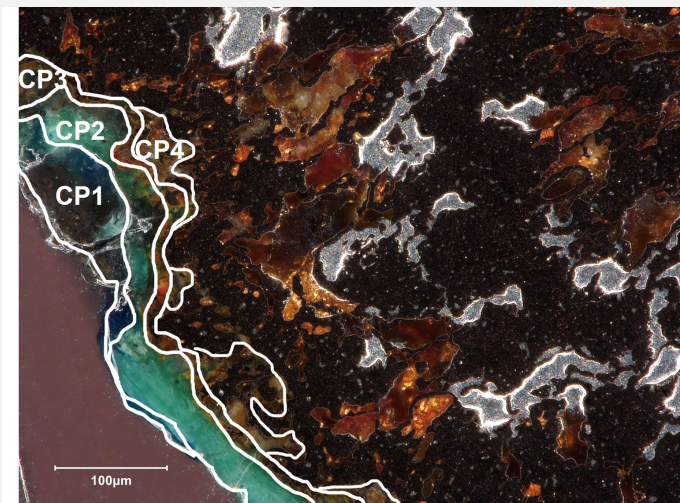
The observation of the sample in cross-section in dark field mode shows the presence of an external blue CP1 layer with sand inclusions, on top of a turquoise CP2 layer, then a red thin internal CP3 layer and an orange CP4 also present in the inclusions inside the corroded metal (Fig. 10).

The EDX elemental analysis (Table 4, Fig.11) of the visually identified CPs by cross-sectional observation shows that the external CP1 and CP2 are Cu-based products with only few amounts of lead (3 wt %), while the orange CP4 is a lead-based compound.

μ-Raman analyses were performed on the identified strata when possible (Fig. 12). The R12 point of analysis was performed on the blue CP1 layer and the corresponding spectrum presented the typical main peaks of azurite ($\text{Cu}_3(\text{CO}_3)_2(\text{OH})_2$). The R9 point of analysis in the green CP2 layer shows the typical peaks of malachite ($\text{Cu}_2(\text{CO}_3)(\text{OH})_2$). The R11 point of analysis was performed on the red thin CP3 layer and shows the main peaks of cuprite (Cu_2O), while the R10 point of analysis was performed on the internal orange corrosion products and showed the typical peaks of litharge (PbO).

Elements	CP1	CP2	CP4
O	29	29	5
Cu	68	69	1
Pb	3	3	94

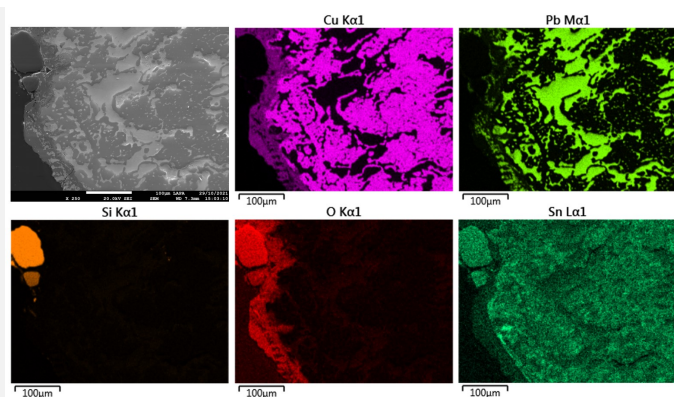
Table 4: Chemical composition (wt %) of the corrosion layers over a general area of analysis in cross-section, LMC-IRAMAT-CNRS-UTBM.



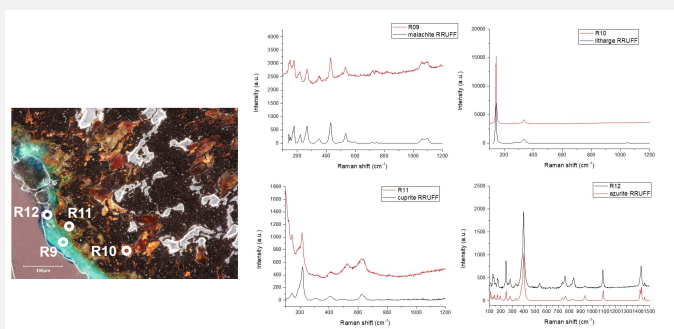
Credit LMC-CNRS, V.Valbi.

Fig. 10: Micrograph of the corrosion structure from Fig. 6 (detail) with the subdivision of the different strata, unetched, dark field,

Fig. 11: SEM image, BSE-mode, and elemental chemical distribution of Fig. 10,



Credit LMC-CNRS, V.Valbi.



Credit LMC-CNRS, V.Valbi.

Corrosion form Multiform - selective

Corrosion type None

Complementary information

None.

✧ MiCorr stratigraphy(ies) – CS

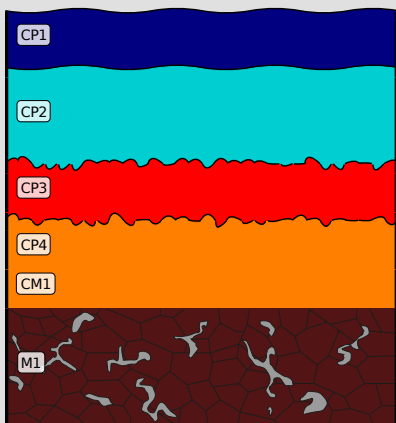


Fig. 13: Stratigraphic representation of the sample of the coin CDN 2012-1-55 observed in cross-section under dark field using the MiCorr application. The characteristics of the strata are only accessible by clicking on the drawing that redirects you to the search tool by stratigraphy representation. This representation was build according to Fig. 10, Credit LMC-CNRS, V.Valbi

✧ Synthesis of the binocular / cross-section examination of the corrosion structure

The stratigraphies obtained by binocular and cross-section observation show a few differences that can be attributed to the different scales of observation. Under binocular microscope, it is possible to differentiate strata according to

texture and light colour changes that do not always correspond to changes in chemical composition, thus leading to a regrouping of several strata into one according to the cross-section observation and physicochemical characterization.

Strata S1 observed in binocular mode is lacking in cross-section observation, probably due to a different observation location. The CP1 and CP2 layers observed under binocular microscope probably correspond to the CP1 and CP2 observed in cross-section, but with the green and the blue layer inversed. The blue CP2 layer observed in binocular mode could correspond to the blue CP1 observed in cross-section and the green CP1 in binocular to the green CP2 in CS. This could be explained as well by the different locations of the observations carried out. Finally, the red cuprite CP3 and the orange litharge CP4 observed in cross-section as well as the corroded metal strata CM1 observed in cross-section were not clearly identified by binocular observation. Still, they could be linked to the black CP3 layers that can not be linked with certainty to any stratum in cross-section, but probably a regrouping of CP3, CP4 and CM1. The binocular view rarely allows documenting CM stratum, as the transition between layers is difficult to assess. M1 could be documented with great accuracy in cross-section and gives multiple information about the internal structure of the metal.

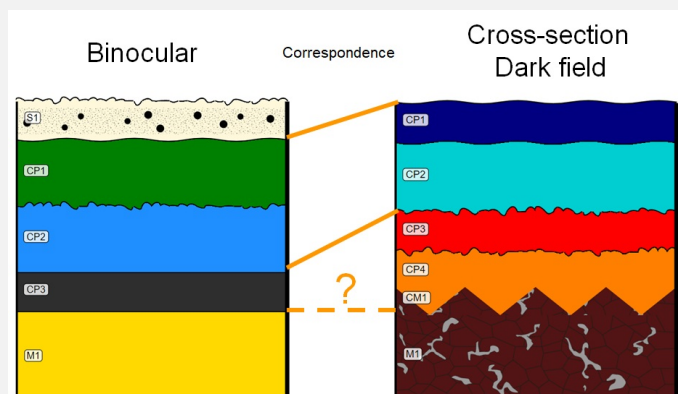


Fig. 14: Stratigraphic representation side by side of binocular view and cross-section (dark field),

Credit LMC-CNRS, V.Valbi/HE-Arc CR, N.Gutknecht.

Conclusion

The coin is composed of a Cu-Pb-Sn ternary bronze alloy with high Pb percentages (29 wt%). Pb is not soluble in the metallic structure and large lead inclusions are observed throughout the whole metal thickness. The metallic microstructure reveals that the object underwent cold working. The whole object is fragilised by the presence of longitudinal cracks filled with corrosion products.

The external corrosion products are composed of Cu-based hydroxycarbonate (azurite and malachite) formed by redeposition of copper with the carbonate ions from the burial environment. Cuprite (Cu_2O) is also identified at the metal interface and is the first corrosion product usually formed on copper-based alloys, while litharge (PbO) is observed in the corroded metal stratum, replacing the lead inclusions selectively attacked.

This coin is part of a corpus of coins found on the same site and called "Peney hoard". Two more coins were studied and have a MiCorr artefact sheet.

References

References on object and sample

1. MiCorr_Coin CdN 2012-1-50
2. MiCorr_Coin CdN 2012-1-57

References on analytical methods and interpretation

3. Lafuente, B., Downs, R. T., Yang, H., Stone, N. (2015) The power of databases: the RRUFF project. In: Highlights in Mineralogical Crystallography, T. Armbruster and R. M. Danisi, eds. Berlin, Germany, W. De Gruyter, 1-30.
4. Scott, D. (2006) Metallography and microstructure of ancient and historic metals. J Paul Getty Museum Publications.
5. Robbiola, L., Blengino, M., Fiaud, C. (1998) Morphology and mechanisms of formation of natural patinas on archaeological Cu-Sn alloys. Corrosion Science, 40 (12), 2083-2111.

